Journal of Materials Chemistry A

PAPER

Phase behavior and superprotonic conductivity in the $Cs_{1-x}Rb_xH_2PO_4$ and $Cs_{1-x}K_xH_2PO_4$ systems

Cite this: *J. Mater. Chem. A*, 2014, **2**, 204

Ayako Ikeda,[a] Daniil A. Kitchaev[b] and Sossina M. Haile*[ab]

Received 27th September 2013
Accepted 8th November 2013

DOI: 10.1039/c3ta13889e

www.rsc.org/MaterialsA

The solid acid compound CsH_2PO_4 (CDP) adopts a cubic structure of high conductivity above 228 °C, rendering it attractive as a fuel cell electrolyte for intermediate temperature operation. This superprotonic phase is stable from the phase transition temperature, T_s, to the dehydration temperature, T_d, where the latter depends on water vapor pressure (*e.g.* T_d = 290 °C at p_{H_2O} = 0.8 atm). In this work we examine the possibility of modifying these temperatures and thereby, amongst other characteristics, fuel cell operating conditions by introduction of Rb and K as substituents for Cs in CDP. The phase behavior of the $Cs_{1-x}Rb_xH_2PO_4$ and $Cs_{1-x}K_xH_2PO_4$ pseudo-binary systems are determined by *in situ* X-ray diffraction (XRD) and thermal analysis. It is found that RbH_2PO_4 (RDP) and CDP are entirely miscible both below and above the transition to the cubic phase. With increasing Rb concentration, T_s increases and T_d decreases. In contrast, K has limited solubility in CDP, with a 27 at.% solubility limit in the cubic phase, and both T_s and T_d decrease with K content. The eutectoid temperature in the $Cs_{1-x}K_xH_2PO_4$ system is 208 ± 2 °C and the K solubility decreases sharply below this temperature. In both systems, conductivity decreases monotonically with increasing substituent concentration. Furthermore, even after normalization for cation size, the impact of K is greater than that of Rb, suggesting local disruptions to the proton migration pathway, beyond global changes in unit cell volume. Although this investigation shows unmodified CDP to remain the optimal fuel cell electrolyte material, the study provides a possible framework for elucidating proton transport mechanisms in superprotonic conductors.

1. Introduction

At moderate temperatures and under sufficient humidity, CsH_2PO_4 adopts the CsCl structure type with orientationally disordered oxyanion groups and has high protonic conductivity ($\sim 10^{-2}$ S cm^{-1}). As such, it is attractive as a fuel cell electrolyte for operation in the intermediate temperature range of 230 to 280 °C.[1–3] In an earlier publication we reported the thermodynamic phase stability of cubic CsH_2PO_4 and the kinetic characteristics of its dehydration.[4] The lower temperature limit for operation of CsH_2PO_4-based fuel cells corresponds to the phase transition temperature, T_s = 228 °C, from the monoclinic to the cubic phase. This polymorphic phase transition is independent of p_{H_2O}. The upper temperature limit corresponds to the dehydration temperature, T_d, which, in contrast to T_s, depends strongly on p_{H_2O}. For example, at p_{H_2O} = 0.8 atm T_d is 290 °C, whereas at p_{H_2O} = 0.15 atm it is 230 °C. The relatively narrow stability window for cubic CsH_2PO_4 presents challenges for fuel cell operation. While these are not insurmountable, increasing T_d and lowering T_s are technologically desirable.[3] In this work we evaluate phase behavior in the $Cs_{1-x}Rb_xH_2PO_4$ and $Cs_{1-x}K_xH_2PO_4$ pseudo-binary systems and explore the possibility of manipulating the stability window of the cubic phase through chemical modification. Beyond near-term implications for fuel cell operation, such a study has the potential to provide broad insight into the crystal-chemical factors governing superprotonic behavior.

At ambient conditions, CsH_2PO_4 and RbH_2PO_4 have distinct structures (the former monoclinic, $P2_1/m$,[5] the latter tetragonal, $I\bar{4}2d$[6]), precluding the possibility of complete solid solubility. It has been shown, however, that Rb is highly soluble in monoclinic CsH_2PO_4, with a solubility limit in the vicinity of 80 at.% at ambient temperatures.[7–9] In addition, it has recently been shown that, upon heating, RbH_2PO_4 transforms to a monoclinic phase isostructural to that of CsH_2PO_4, with the transition occurring gradually over the temperature range from 90 to 130 °C.[10] In the case of the intermediate compositions, a sharp increase in conductivity on heating to somewhat higher temperatures,[7–9,11] as well as observation of a thermal anomaly of appropriate magnitude,[8,12] has suggested that $Cs_{1-x}Rb_xH_2PO_4$ can adopt the cubic CsCl-type structure of superprotonic CsH_2PO_4. Direct high-temperature diffraction studies are limited to the work of Martsinkevich,[13] who was able to show that for compositions up to 40 at.% Rb the high-temperature phase is indeed cubic. In parallel with these

[a]*Materials Science, California Institute of Technology, 1200 E. California Blvd, Pasadena, CA 91125, USA. E-mail: smhaile@caltech.edu*

[b]*Chemical Engineering, California Institute of Technology, 1200 E. California Blvd, Pasadena, CA 91125, USA*

ambient pressure experiments, Botez examined RbH_2PO_4 under high pressure and reported the occurrence of monoclinic and cubic phases of RbH_2PO_4, isostructural with those of CsH_2PO_4.[14] This collection of prior results suggests the possibility of complete miscibility between CsH_2PO_4 and RbH_2PO_4 at temperatures in the vicinity of T_s, below it in the form of the monoclinic phase and above in the form of the cubic phase. Studies of the impact of Rb substitution on the temperature of the transition between these two phases generally indicate an increase in T_s with increasing Rb,[7–9,12,15] although Lavrova *et al.* have reported a 20 °C reduction in T_s when the Rb content is 3 at.%.[11] Little has been documented with respect to the influence of Rb on dehydration behavior. We reported previously that $Cs_{0.75}Rb_{0.25}H_2PO_4$ has a slightly lower T_d than CsH_2PO_4.[12] Again, Lavrova *et al.* have reported opposite behavior, claiming enhanced stability for $Cs_{0.97}Rb_{0.03}H_2PO_4$ over CsH_2PO_4.[11] These discrepancies signify a clear need to resolve the phase behavior of the $Cs_{1-x}Rb_xH_2PO_4$ system and quantify the influence of Rb content on T_s and T_d.

In contrast to the case with Rb, there are no known studies of the $Cs_{1-x}K_xH_2PO_4$ system. At ambient temperatures, KH_2PO_4 is tetragonal[16] and isostructural to the ambient temperature form of RbH_2PO_4. Recent high-temperature synchrotron X-ray studies[17] have revealed a transition at ~190 °C to a monoclinic phase ($P2_1/m$), isostructural to that of RbH_2PO_4 (above 130 °C) and CsH_2PO_4 (ambient temperature). However, further heating apparently results in melting or dehydration prior to any transition to a superprotonic phase, even under high pressure.[18] Because K is only slightly smaller than Rb and the phosphates share two isomorphous structures, non-negligible solubility of K into CsH_2PO_4 can be anticipated, suggesting another chemical means of manipulating T_s and T_d in CsH_2PO_4-based materials.

To meet the objective of elucidating phase behavior we perform, in this work a careful examination of the $Cs_{1-x}Rb_xH_2PO_4$ and $Cs_{1-x}K_xH_2PO_4$ pseudo-binary systems using *in situ* X-ray powder diffraction (XRD), differential scanning calorimetry (DSC) and alternating current (AC) impedance spectroscopy. Key to the success of this study is the active control of humidity in order to clearly distinguish between polymorphic phase transitions and dehydration reactions,[19] as well as acquisition of data over long periods to ensure system equilibration. This approach enables reliable determination of (i) solubility limits, (ii) T_s, and (iii) T_d, all of which are embodied in the phase diagrams constructed from these measurements.

2. Experimental details

2.1. Sample preparation

Polycrystalline powders of CsH_2PO_4 and RbH_2PO_4 were synthesized by combining the starting reagents Cs_2CO_3 (Alfa Aesar, 99.99%) or Rb_2CO_3 (Alfa Aesar, 99.99%) and H_3PO_4 (ACS, 85% w/w aqueous solution) in a molar ratio of 1 : 2 in aqueous solution. The resulting solutions were gently heated and the end-member solid acid phosphates obtained upon evaporation of water. Samples of overall composition $Cs_{1-x}Rb_xH_2PO_4$ and $Cs_{1-x}K_xH_2PO_4$ were synthesized from these starting materials.

Table 1 Rb concentration in $Cs_{1-x}Rb_xH_2PO_4$ samples as determined by EDS

Sample	Nominal (at.%)	Measured (at.%)
19%Rb	20	19.4 ± 1.2
50%Rb	50	50.1 ± 1.3
78%Rb	75	77.8 ± 1.8

Stoichiometric aqueous solutions of target overall composition were prepared and again solid precipitates obtained upon inducing water evaporation. For further experimentation the resulting materials were ground in a mortar and pestle to yield to powders with particle size of ~10 μm.

Chemical compositions were measured by X-ray energy dispersive spectroscopy (EDS), performed using an Oxford INCA 300 in conjunction with a scanning electron microscope (LEO 1550 VP) at an accelerating voltage of 15 kV. For the $Cs_{1-x}Rb_xH_2PO_4$ system, slight differences were determined between the nominal and actual compositions, Table 1, and all results are presented in terms of the actual (measured compositions). In the case of the $Cs_{1-x}K_xH_2PO_4$ system, the solubility of K into CsH_2PO_4 was found to be extremely limited, and the multi-phase nature of the resulting materials prevented acquisition of meaningful EDS data. Consequently, for these materials we refer only to the nominal compositions.

2.2. *In situ* XRD measurements

XRD measurements were carried out using an X'pert MD (Panalytical) diffractometer equipped with an in-house constructed sealed, high-temperature stage, Fig. 1. Two resistive heaters in the sample stage provide heat to the sample, the temperature of which is monitored and controlled using a thermocouple (K-type) also embedded in the stage. Three additional resistive heaters, typically set to ~150 °C, are embedded in the walls of the chamber and are utilized to

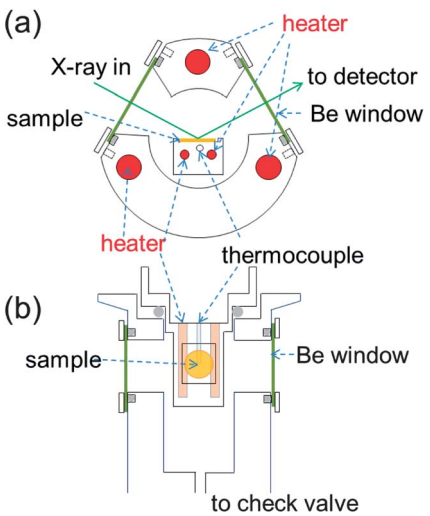

Fig. 1 Schematic illustration of the sealed, high-temperature X-ray powder diffraction stage constructed for data collection under high p_{H_2O}, up to 2 atm: (a) cross-sectional view, and (b) top-down view.

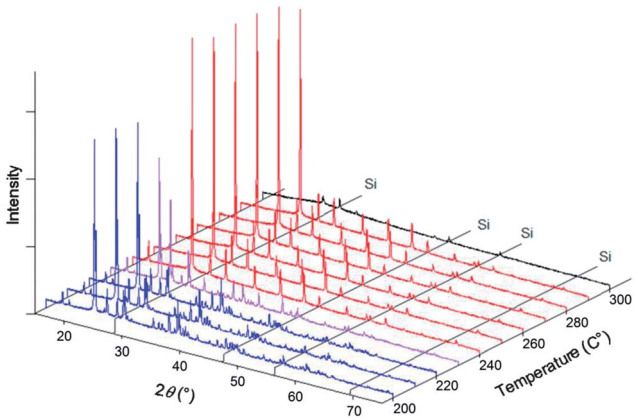

Fig. 2 XRD patterns of CsH_2PO_4 with Si (as an internal standard) at several temperatures showing wide temperature range of stability of the cubic phase (red patterns) under sufficiently high humidity, estimated to be ~1 atm.

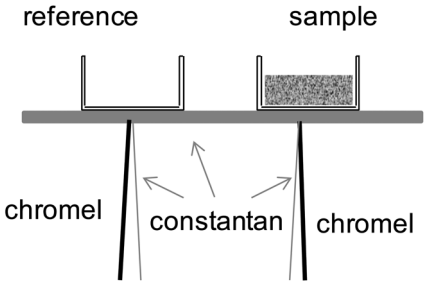

Fig. 3 Schematic illustration of the in-house constructed DSC cell used for thermal studies under high p_{H_2O}.

prevent water condensation. The chamber is further equipped with a check valve to limit the system pressure to 2 atm. Be windows permit incident and diffracted X-rays to enter and exit the chamber. A thin glass plate was placed on the sample stage to prevent possible reaction between the sample and stage material. The sample powder was combined, by light mechanical milling, with 20 at.% Si (Alfa Aesar, 99.9%), which served as an internal 2θ reference. No reaction between Si and the materials investigated was observed. Measurements were typically carried out in the temperature range 150 to 300 °C in 10 °C increments. Samples were held at each temperature for at least 30 minutes prior to data acquisition to allow for equilibration.

Exemplary diffraction data obtained from this system are presented in Fig. 2 for the parent compound CsH_2PO_4. Consistent with the widely confirmed phase transformation behavior, the data show CsH_2PO_4 to remain entirely in the monoclinic phase to 220 °C. A two-phase mixture of the monoclinic and cubic phases is obtained at 230 °C, and from 240 to 290 °C only diffraction peaks from the cubic phase are evident. The material becomes entirely amorphous at 300 °C, corresponding to the occurrence of a liquid phase, likely as a result of direct melting. Based on the retention of the cubic phase to such high temperature,[19] we estimate that a water partial pressure of ~1 atm was attained in the sealed chamber. Crystallographic parameters were determined by Rietveld refinement using the RIETAN-FP software package.[20] The known thermal expansion behavior of Si (ref. 21) provided an internal 2θ standard to ensure accurate lattice parameter refinement. To facilitate refinement of atomic positions, the P–O distance was fixed (at 1.52 Å (ref. 8)) irrespective of temperature. The refined parameters for cubic CsH_2PO_4 ($Pm\bar{3}m$) are presented in Table 2.

2.3. Thermal measurements

Thermal analysis was performed using an in-house constructed differential thermal analyzer, shown schematically in Fig. 3, capable of accessing temperatures as high as 350 °C (with 0.1 °C stability) under water partial pressures as high as 0.9 atm. The system is a modification to an apparatus described previously as part of our earlier study of the phase behavior of CsH_2PO_4.[4] In the present design, the sample stage is constructed of constantan alloy, the reference and sample are placed on the stage as shown in the figure, and directly beneath each (on the opposite side of the stage) is welded the junction of an E-type thermocouple. The temperatures of the sample and thermocouple are measured directly using the thermocouples, whereas the differential thermal signal between the sample and the reference is additionally recorded *via* measurement of the voltage generated between the two chromel leads. The voltage data are collected using a nanovolt meter (Keithley 182) with ±100 nV accuracy, corresponding to a precision of 0.02 mW. The electrical paths for measuring absolute temperature (the voltage between chromel–constantan couples) and that for measuring the differential temperature (voltage between two chromel leads) were electrically isolated during measurements

Table 2 Rietveld refinement fit parameters for cubic CsH_2PO_4 ($Pm\bar{3}m$, CsCl structure type) at several temperatures

		Cs1					P1					O1						
T (°C)	a_0 (Å)	sof	x	y	z	B	sof	x	y	z	B	sof	x	y	z	B	S	R_p
230	4.9673(9)	1	0	0	0	8.2	1	1/2	1/2	1/2	4.4	0.1667	1/2	0.221	0.374	4.4	—	—
240	4.9683(2)	1	0	0	0	8.2(1)	1	1/2	1/2	1/2	4.4(2)	0.1667	1/2	0.221(1)	0.374(1)	4.4(2)	1.38	3.94
250	4.9707(2)	1	0	0	0	8.7(1)	1	1/2	1/2	1/2	4.9(2)	0.1667	1/2	0.222(1)	0.374(2)	4.9(2)	1.32	3.79
260	4.9728(2)	1	0	0	0	8.7(1)	1	1/2	1/2	1/2	4.8(2)	0.1667	1/2	0.222(1)	0.373(2)	4.8(2)	1.34	3.80
270	4.9748(2)	1	0	0	0	8.9(1)	1	1/2	1/2	1/2	4.7(2)	0.1667	1/2	0.223(1)	0.374(1)	4.7(2)	1.30	3.77
280	4.9764(2)	1	0	0	0	9.3(1)	1	1/2	1/2	1/2	4.9(2)	0.1667	1/2	0.223(1)	0.367(2)	4.9(2)	1.31	3.80
290	4.9777(2)	1	0	0	0	9.4(1)	1	1/2	1/2	1/2	6.0(2)	0.1667	1/2	0.222(1)	0.374(1)	6.0(2)	1.18	3.49

by switching from one circuit to the other using a by Keithley 7001. The magnitude of the differential thermal signal was calibrated for measurement of heat using the melting reactions of Sn and of Pd at 232 and 327 °C, respectively. The heating and humidification schemes are unchanged relative to the previous configuration.[4]

Prior to examination, the sample powders were combined with 20 wt% amorphous silica powder (Alfa Aesar, S.A 330–410, 325 mesh), homogenized by mechanical agitation, and then annealed under high humidity (p_{H_2O} = 0.6–0.85 atm) at high temperature (2 h at 350 °C followed by 6 h at 250 °C). This treatment creates a composite sample with a fine structure, which accelerates dehydration and hydration kinetics[4] and enables access to equilibrium behavior on laboratory time scales.

Thermal data were collected at a heating rate of 0.5 K min^{-1} using samples typically 60 mg in mass. Under these conditions, the enthalpy for the superprotonic phase transition, with a reported value of 11.6 kJ mol,[19] is detected as 11.5 ± 0.6 kJ mol^{-1}. Due to the excellent quantitative agreement, the method can be considered functionally identical to differential scanning calorimetry (DSC).

2.4. AC impedance measurements

Conductivity of the materials was determined by AC impedance spectroscopy (HP 4284A). Samples were formed into discs, 9.3 mm in diameter and typically 2 mm in thickness, by uniaxial pressing of ground powders at 491 MPa for 10 min to achieve a relative density of 99% as determined from direct measurements of mass and physical dimensions. Sputtered films of Pt or Ag, approximately 100 nm in thickness, served as electrodes. Samples were placed in a horizontal tube furnace and held in place using Pt wire current collectors. Measurements were carried out in the temperature range 180 to 280 °C under humidified N_2, p_{H_2O} = 0.9 atm, achieved by passing the inlet gas through a water bubbler held at 98 °C prior to its entrance to the measurement zone. Step changes in temperature of 5 to 10 °C were applied and the system allowed to equilibrate for at least 30 minutes or until the impedance response had stabilized before recording the final data. The temperature was measured using an alumina sheathed E-type thermocouple placed in direct contact with the sample.

3. Results and discussion

3.1. Overall phase characteristics

Integration of the results of the comprehensive structural, thermal and transport measurements of the materials yielded the phase diagrams presented in Fig. 4, part (a) showing the CsH_2PO_4–RbH_2PO_4 system and (b) the CsH_2PO_4–KH_2PO_4 system. Circles designate phase transition temperatures, squares dehydration temperatures, and triangles phase boundaries, where data in blue were acquired by DSC measurements and those in black by *in situ* XRD measurements. The CsH_2PO_4–RbH_2PO_4 system has simple isomorphous phase behavior. The end-members are entirely miscible at temperatures above 150 °C in both the monoclinic and cubic phases. The superprotonic transition temperature increases monotonically and the dehydration temperature largely decreases with increasing Rb content, resulting in a narrowing of the superprotonic region. At ambient temperature (not shown) the solubility limit of Rb into CsH_2PO_4 is ~80 at.%,[8] and the transformation of RbH_2PO_4 into the CsH_2PO_4-like monoclinic phase at 117 °C (ref. 22) facilitates complete solid solubility at the temperatures probed in this study. While compositions with very low Rb content were not explicitly studied here, the generally smooth manner in which the phase boundaries vary with composition suggest that the remarkable stabilization observed by Lavrova[11] for $Cs_{0.97}Rb_{0.03}H_2PO_4$ may have been an artifact due to kinetic effects.

In sharp contrast to the CsH_2PO_4–RbH_2PO_4 system, the CsH_2PO_4–KH_2PO_4 system displays eutectoid behavior with limited solubility of K in either phase of CsH_2PO_4. On introduction of K, the superprotonic transition temperature shifts

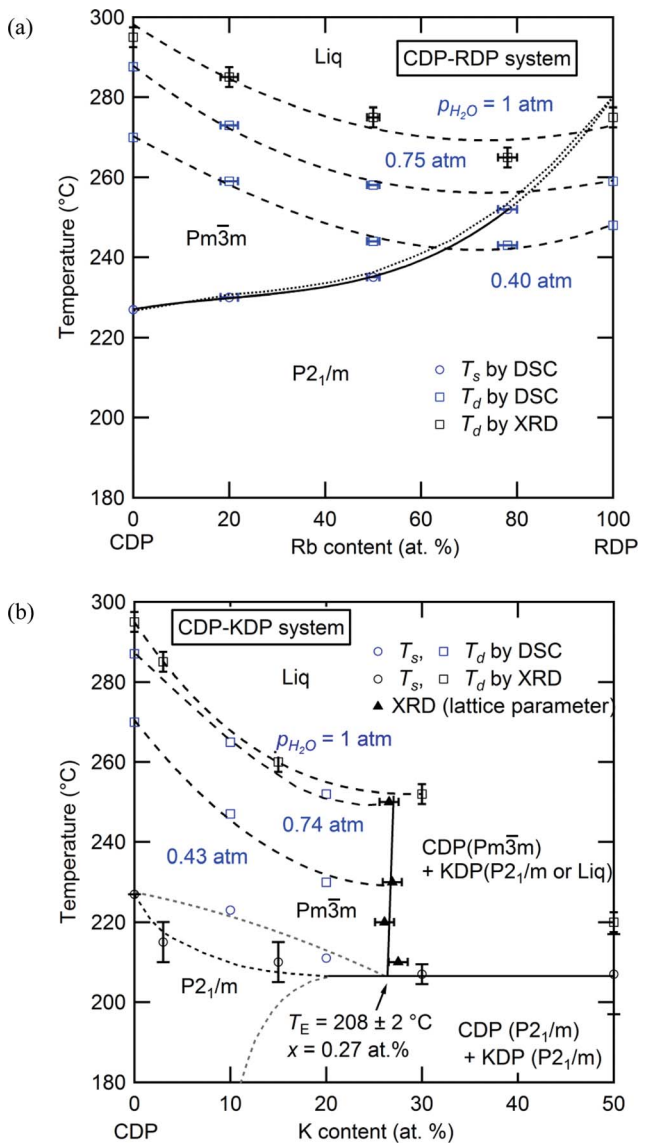

Fig. 4 Phase diagrams of the (a) CsH_2PO_4–RbH_2PO_4, and (b) CsH_2PO_4–KH_2PO_4 systems. The dashed curves indicate the dehydration temperatures at the given values of p_{H_2O}. The solid and dotted curves are phase boundaries.

downward until the eutectoid temperature of ~208 °C (20 °C lower than the superprotonic temperature of neat CsH_2PO_4) is reached. The solubility of K into cubic CsH_2PO_4 is 27 at.% and is surprisingly temperature insensitive above the eutectoid point. Due to the challenges of determining composition *in situ* at high temperature, the solidus and solvus lines, however, could not be accurately determined; the dotted and dashed lines are approximate locations for these boundaries based on the requirements of the Gibbs phase rule.[23] At ambient temperature (not shown in the phase diagram) the solubility of K into monoclinic CsH_2PO_4 is just 7.2 ± 0.8 at.%, significantly lower than the 27 at.% at the eutectoid point. Above the eutectoid temperature, compositions with greater than 27 at.% K form a mixture of a cubic CDP-rich phase and a KH_2PO_4-rich phase. At moderate temperatures the latter adopts the crystalline monoclinic structure recently reported for neat KH_2PO_4 (ref. 17) and transforms to a liquid at higher temperatures. The precise transformation temperature, which was found to be sensitive to humidity, could not be determined as a result of sluggish kinetics. Overall, the dehydration temperature in this system decreases notably on introduction of K, particularly so within the single-phase superprotonic region. Accordingly, there is an overall shift of the stable cubic region to lower temperature with increasing K content, along with a slight narrowing of the stability window.

3.2. Determination of phase behavior in the $Cs_{1-x}Rb_xH_2PO_4$ system: $0 \leq x \leq 1$

In situ XRD data were collected for the specific compositions in the $Cs_{1-x}Rb_xH_2PO_4$ system of $x = 0.19$, 0.5, 0.78 (the actual compositions, Table 1) and for the end-member RbH_2PO_4, in addition to CsH_2PO_4 as reported above. Example diffraction results are presented in Fig. 5 both as a function of composition (part a) at high temperature ($T = 260$ °C) and as a function of temperature (parts b and c) for given compositions ($x = 0.5$, 1, respectively). The data show that the $Cs_{1-x}Rb_xH_2PO_4$ compounds transform from the CDP-type monoclinic phase to the cubic CsCl-type phase of superprotonic CsH_2PO_4. Furthermore, the monoclinic $P2_1/m$ phase reported to occur above 130 °C in RbH_2PO_4 is confirmed (and is even found to exist at 120 °C). However, no cubic phase was observed in the absence of Cs. The diffraction peaks are lost from RbH_2PO_4 at 270 °C, suggesting the occurrence of a liquid phase. It is possible the cubic superprotonic phase may be accessible under p_{H_2O} values higher than the ~1 atm estimated for the sealed diffraction chamber, as it is under high total pressure (1 GPa).[14] Such conditions were not examined here. For all the compounds, at sufficiently high temperatures, the XRD data are marked by the absence of diffraction peaks. By analogy to CsH_2PO_4, this behavior is taken to reflect the presence of a partially dehydrated liquid ($MH_{2-2x}PO_{4-x}$(l), M = alkali metals), and the temperature at which the crystalline phase is no longer observed is taken to be the decomposition temperature. Weight loss at this temperature was not independently confirmed, but the DSC measurements, as discussed below, are consistent with such an interpretation.

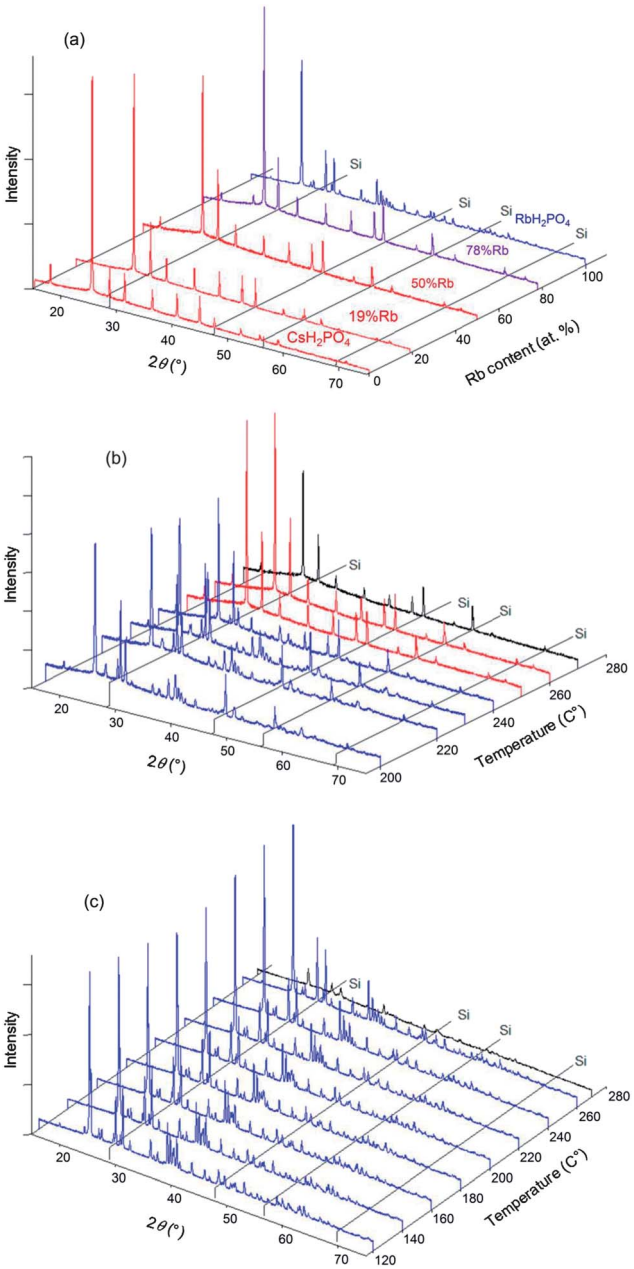

Fig. 5 Selected XRD patterns obtained in the $Cs_{1-x}Rb_xH_2PO_4$ system with Si (as internal standard). (a) Results at 260 °C with various *x*; and results at (b) $x = 0.5$ and (c) $x = 1.0$ (RbH_2PO_4), as functions of temperature. Red patterns correspond to the cubic phase ($Pm\bar{3}m$), blue patterns to the monoclinic phase ($P2_1/m$) and purple patterns to 2-phase mixtures. Patterns shown in black are those with lower intensity due to amorphization and/or melting. Selected XRD patterns obtained in the $Cs_{1-x}Rb_xH_2PO_4$ system.

Selected DSC profiles for compounds in the $Cs_{1-x}Rb_xH_2PO_4$ system are presented in Fig. 6, part a for fixed $x = 0.19$ and part b for fixed p_{H_2O}. Two thermal events are evident in all cases. At fixed stoichiometry, the first event occurs at a given temperature, 230 °C in this example, whereas the second depends on the water partial pressure. This behavior is consistent with the identification of the first transition as a polymorphic transformation, involving no change in sample composition, and of

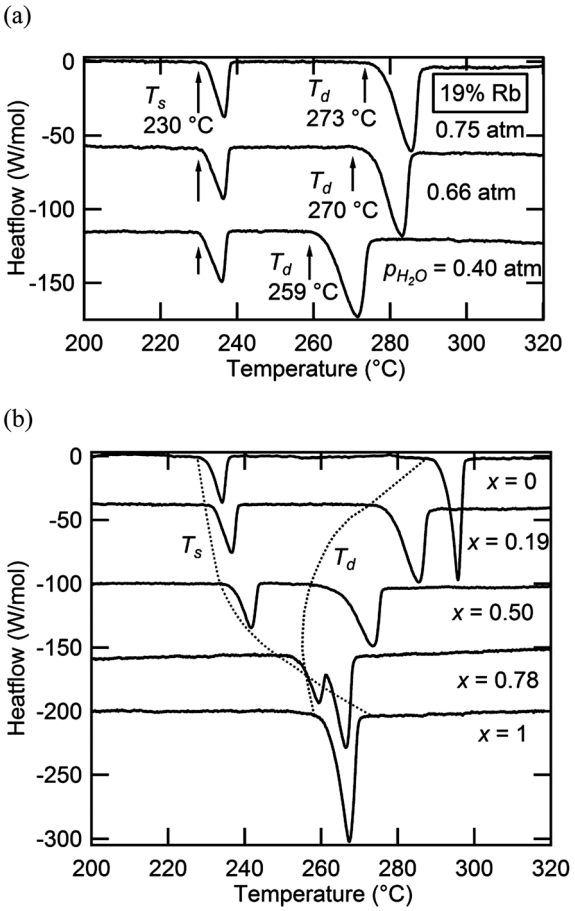

Fig. 6 Selected DSC profiles of materials in the $Cs_{1-x}Rb_xH_2PO_4$ system: (a) results as a function of p_{H_2O} at fixed composition ($x = 0.19$); and (b) results as a function of composition at fixed p_{H_2O} (0.75 atm).

the second transition as a dehydration or partial dehydration event, involving loss of H_2O from the structure. With increasing Rb content (Fig. 6b), the temperature of the polymorphic transition monotonically increases, whereas the decomposition temperature generally decreases but finally increases slightly for the RbH_2PO_4 end-member. At $x = 0.78$ and $p_{H_2O} = 0.75$ atm, for example, the polymorphic transition just precedes the dehydration, and the two events are almost indistinguishable. These trends are reflected in the phase diagram presented in Fig. 4(a), for which T_s and T_d are defined in terms of the onset of the respective thermal anomalies.

In principle, the monoclinic to cubic phase transition should pass through a two-phase region. The relatively sharp DSC peaks, spanning no more than ~9 K, indicate that the two-phase region is rather narrow, as displayed in the phase diagram. No attempt was made in the diffraction measurements to capture the compositional breadth of the two phase region, a rather subtle feature of the phase diagram. Similar to the superprotonic transition, the dehydration anomaly displays a relatively sharp peak, despite the likely transformation to a partially dehydrated liquid and continuous weight loss at high temperature.[4] Such behavior is similar to that observed in CsH_2PO_4 in which the dehydration is confirmed to occur over a wide temperature range but with a relatively sharp thermal signal, reflecting the fact that the majority of the weight loss occurs shortly after the onset of dehydration. The breadths, magnitudes, and onset temperatures for the superprotonic transformation and dehydration peaks are summarized in Table 3. The enthalpies of transformation/dehydration are largely independent of composition, with a typical value of 11.5 kJ mol^{-1} for the superprotonic transition and 31.4 kJ mol^{-1} for dehydration (comparable to the thermal properties of CsH_2PO_4 (ref. 4)). It has been suggested that the entropy of the superprotonic transition can be accounted for in terms of the configurational disorder of the oxygen atoms and protons in the cubic phase.[19,24] In light of the almost constant T_s, an almost constant ΔH is consistent with this interpretation and suggests the absence of any local ordering effects between Cs and Rb.

3.3. Determination of phase behavior in the $Cs_{1-x}K_xH_2PO_4$ system: $0 \leq x \leq 0.5$

The room temperature XRD patterns of the $Cs_{1-x}K_xH_2PO_4$ system have not been previously reported and are accordingly provided here in Fig. 7. The patterns with $x = 0$ and 0.03 are almost identical, indicating a minimum K solubility of 3 at.%. At higher x (10 at.% and higher), the patterns reflect the presence of a two-phase mixture of a CsH_2PO_4-type monoclinic phase ($P2_1/m$) and a KH_2PO_4-type tetragonal phase. From an analysis of the intensity of the diffraction peaks of the latter and extrapolation to the composition at which these peaks would have zero intensity, we estimate the K solubility in monoclinic CsH_2PO_4 to be 7.2 ± 0.8 at.% (Fig. 7b). Within the two-phase region, the lattice constants of the KH_2PO_4-type tetragonal phase are, within error, equal to that of neat KH_2PO_4 (specifically, respective cell volumes of 386.1 (ref. 16) and 384 ± 1 $Å^3$ at

Table 3 Features of the peaks detected in the DSC profiles of $Cs_{1-x}Rb_xH_2PO_4$ alloys

	Superprotonic transition			Dehydration		
Composition	ΔH (kJ mol^{-1})	T_{onset} (°C)	FWHM (°C)	ΔH (kJ mol^{-1})	T_{onset} (°C)	FWHM (°C)
CsH_2PO_4	11.5 ± 0.6	227.2 ± 0.4	2.9 ± 0.1	31.0 ± 1.6	288.5 ± 0.5	2.6 ± 0.1
19%Rb	11.8 ± 0.5	230.6 ± 0.3	3.6 ± 0.1	30.2 ± 1.3	273.5 ± 0.4	5.7 ± 0.1
50%Rb	11.8 ± 0.9	234.9 ± 0.4	3.7 ± 0.1	29.0 ± 3.1	258.1 ± 0.5	6.3 ± 0.1
78%Rb	—	251.6 ± 0.2	4.2 ± 0.1	—	258 ± 3	4.2 ± 0.1
RbH_2PO_4	—	—	—	—	258.9 ± 0.6	4.3 ± 0.1

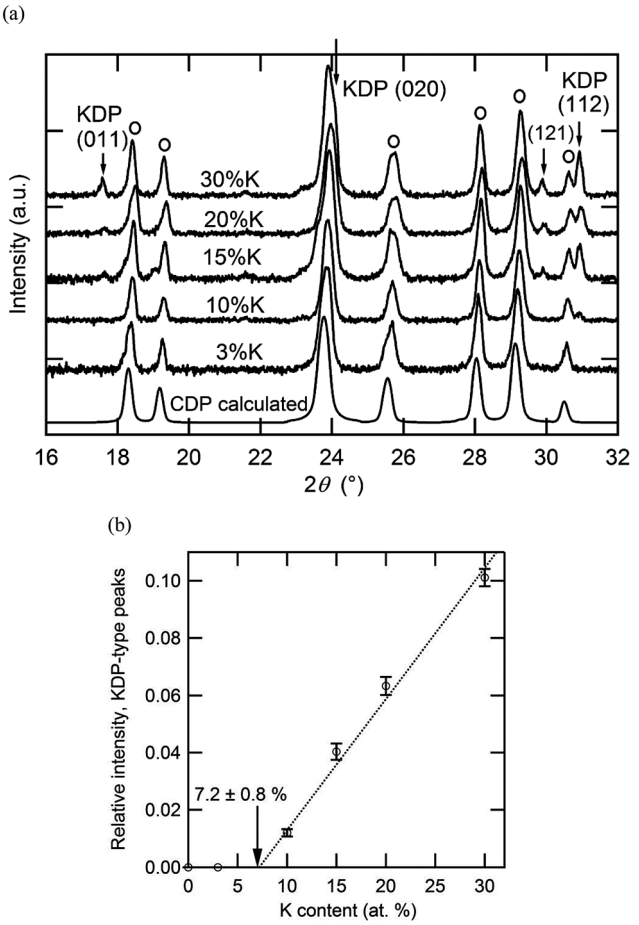

Fig. 7 Room temperature X-ray diffraction analysis of $Cs_{1-x}K_xH_2PO_4$: (a) XRD patterns from compositions with x as specified, and (b) summed intensity of KDP-type peaks {(011), (121) and (112) peaks} relative to the summed intensity of CDP-type peaks identified in (a) by the label O.

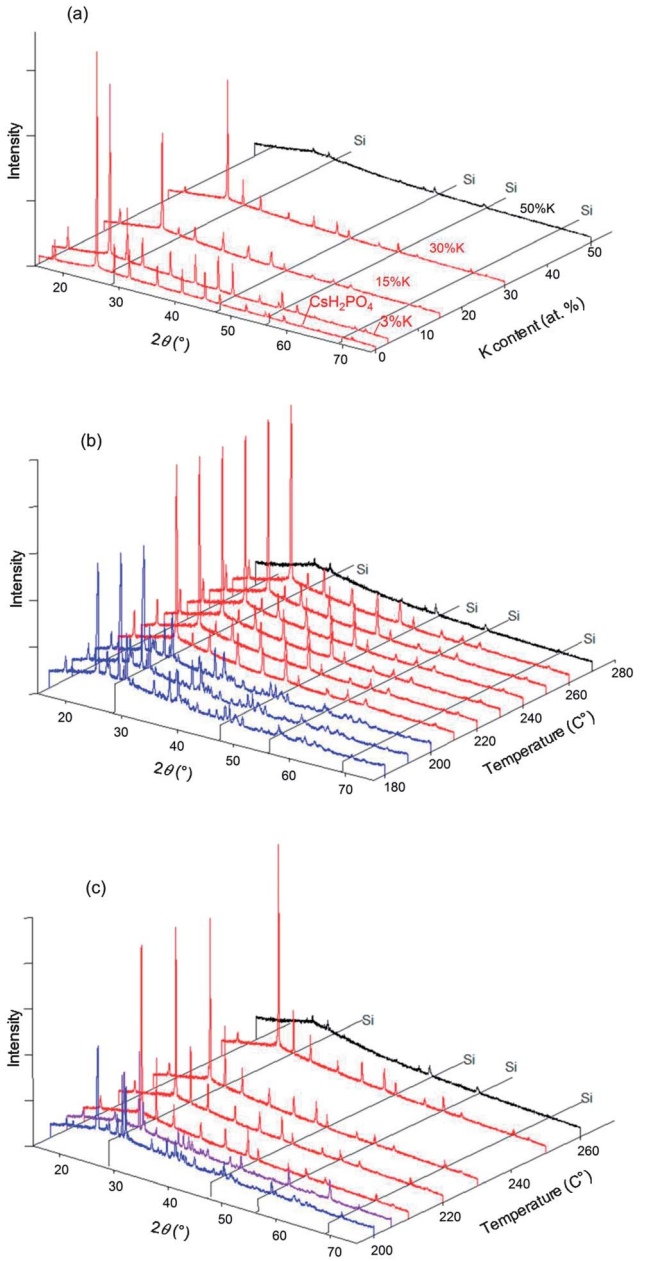

Fig. 8 Selected XRD patterns obtained in the $Cs_{1-x}K_xH_2PO_4$ system with Si (as internal standard). (a) Results at 250 °C with various x; and results at (b) $x = 0.15$ and (c) $x = 0.30$ as functions of temperature. Red patterns correspond to the cubic phase ($Pm\bar{3}m$), blue patterns to the monoclinic phase ($P2_1/m$) and purple patterns to 2-phase mixtures. Patterns shown in black are those with lower intensity due to amorphization and/or melting. Selected XRD patterns obtained in the $Cs_{1-x}K_xH_2PO_4$ system.

room temperature), indicating that the solubility of Cs into this phase is no more than a few at. %.

In situ high-temperature XRD experiments were performed in the $Cs_{1-x}K_xH_2PO_4$ system for the specific compositions $x = 0.03$, 0.15, 0.3, and 0.5, with higher potassium concentrations being of less interest with respect to superprotonic behavior. Selected diffraction results are presented in Fig. 8. At 250 °C, the data show that the cubic CsCl-type phase is the only crystalline phase present for all compositions (Fig. 8a), but in the case of $x = 0.5$, a broad amorphous background, indicative of a liquid phase, is the most significant feature, and the peaks from the crystalline phase are barely detectable. That the amorphous phase is liquid rather than solid was deduced on the basis of the transformation of the loose powder sample placed in the diffraction chamber into a coagulated, shiny agglomerate by the conclusion of the experiments. The temperature-dependent diffraction data reveal the $x = 0.15$ composition to be composed in the temperature range from 180 to 200 °C of a mixture of isostructural CsH_2PO_4-type and KH_2PO_4-type monoclinic phases (Fig. 8b). Lower temperatures were not examined, but this result indicates that, as with the Rb system, dissolution of Cs into KH_2PO_4 stabilizes the monoclinic form otherwise observed at slightly higher temperatures[17] (190 °C and higher). At temperatures between 210 and 260 °C only peaks from the CsCl-type cubic phase are evident, and finally at 270 °C all diffraction peaks disappear and only the liquid is present. This behavior is generally reproduced for the $x = 0.3$ composition (Fig. 8c). In this case, however, an additional peak was observed around $2\theta = 25°$ at temperatures at which the cubic phase is stable, as shown more clearly in Fig. 9. The peak location coincides with

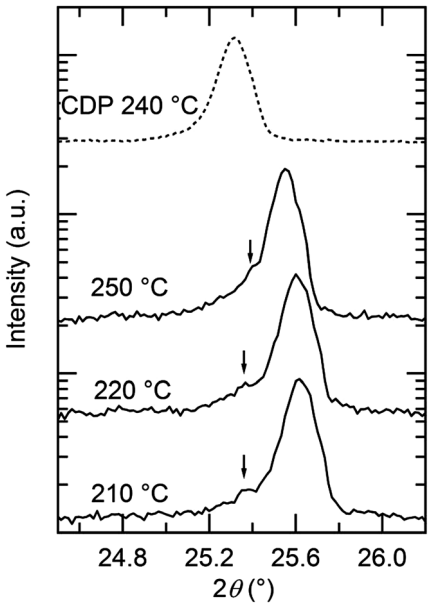

Fig. 9 Exploded view of high-temperature diffraction patterns of $Cs_{0.7}K_{0.3}H_2PO_4$ in the vicinity of the (1 1 $\bar{1}$) peak of the KDP-type monoclinic phase, shown in comparison to the pattern of neat CsH_2PO_4 (top).

that of the (1 1 $\bar{1}$) peak of monoclinic KH_2PO_4. At 205 °C after cooling from 210 °C, peaks from the cubic CsH_2PO_4-type phase, the monoclinic CsH_2PO_4-type phase and the monoclinic KH_2PO_4-type phase were observed. This co-existence suggests that the lower boundary of the cubic CsH_2PO_4-type phase lies between 205 and 210 °C. Slow equilibration kinetics prevented acquisition of diffraction data that would have provided more definitive identification of the phase boundaries.

Given the challenges of direct determination of the equilibrium phase assemblage at high temperature, an evaluation of the lattice parameter dependence on composition was used as a secondary means of estimating the solubility limit of K into cubic $Cs_{1-x}K_xH_2PO_4$. In Fig. 10 this parameter is shown as a function of potassium content at 230 and 250 °C. At low K content, the cell constant decreases linearly, in accord with

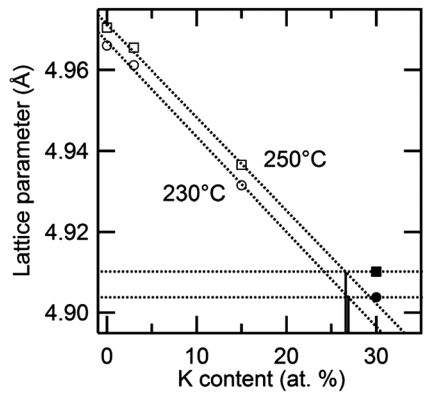

Fig. 10 Variation of the high temperature lattice parameter of cubic $Cs_{1-x}K_xH_2PO_4$ as a function of x at 230 and 250 °C.

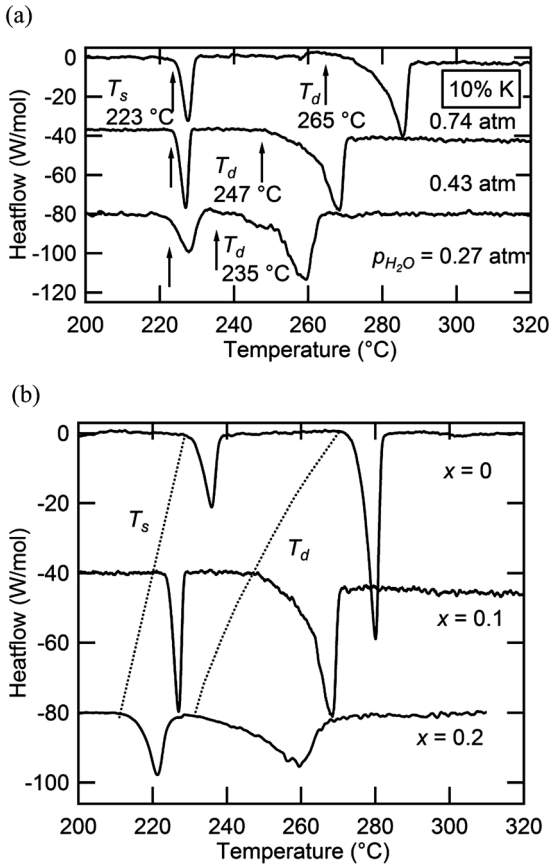

Fig. 11 Selected DSC profiles of materials in the $Cs_{1-x}K_xH_2PO_4$ system: (a) results as a function of p_{H_2O} at fixed composition ($x = 0.10$) and (b) results as a function of composition at fixed p_{H_2O} (0.43 atm).

Vegard's empirical law. The data points for the $x = 0.3$ composition, however, deviate from the linear relationship. Extrapolation of the lattice parameter trendline to the measured values at $x = 0.3$ suggests an actual composition (*i.e.*, solubility limit) of 27 at.% at both temperatures. This method of analysis is justified by the observation of a linear dependence of lattice parameter on dopant content in the superprotonic cubic phase within the $Cs_{1-x}Rb_xH_2PO_4$ system (as discussed below).

Selected DSC measurements in the $Cs_{1-x}K_xH_2PO_4$ system are presented in Fig. 11, showing both (a) isocompositional and (b) isobaric results. Thermal measurements in this case were limited to compositions of $x = 0.1$ and 0.2. As evidenced from Fig. 11(a), a lower temperature transition occurs that is independent of p_{H_2O} and is followed by a higher temperature one that shifts to lower temperature on decrease of p_{H_2O}. These events are consequently interpreted as a polymorphic transition and a dehydration reaction, respectively. The behavior is analogous to that of the $Cs_{1-x}Rb_xH_2PO_4$ system, with the dehydration similarly resulting in a product phase that is a liquid. In contrast to the first system, however, a slight discrepancy was observed with respect to the temperature of the polymorphic transition as determined by diffraction and by calorimetry. For example, for $x = 0.15$, one observes a fully cubic pattern at 210 °C, Fig. 8b, whereas the $x = 0.10$ composition has an onset for the polymorphic transition, T_s, of 223 °C. Furthermore, on

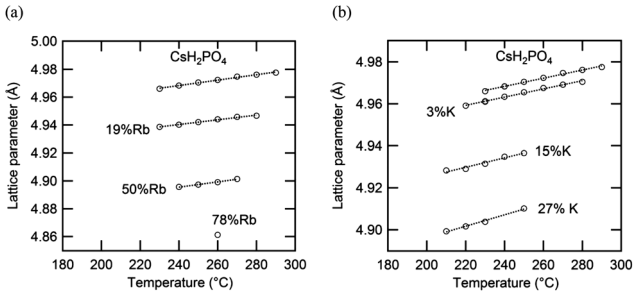

Fig. 12 Lattice parameters of cubic (a) $Cs_{1-x}Rb_xH_2PO_4$ and (b) $Cs_{1-x}K_xH_2PO_4$ as functions of temperature under $p_{H_2O} \sim 1$ atm (the estimated errors lie within the size of the data markers).

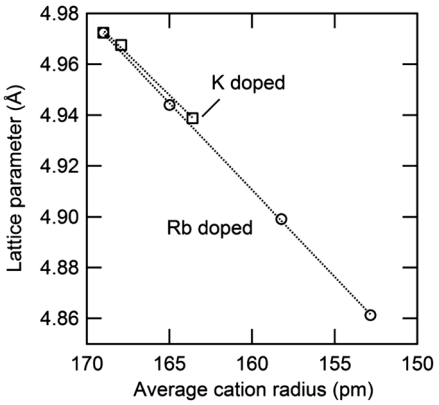

Fig. 13 Relationship between averaged ionic radius and lattice parameter in cubic $Cs_{1-x}Rb_xH_2PO_4$ and $Cs_{1-x}K_xH_2PO_4$ at 260 °C. For the latter, the values are extrapolated from measurements at slightly lower temperatures using the measured thermal expansion coefficient (Table 4).

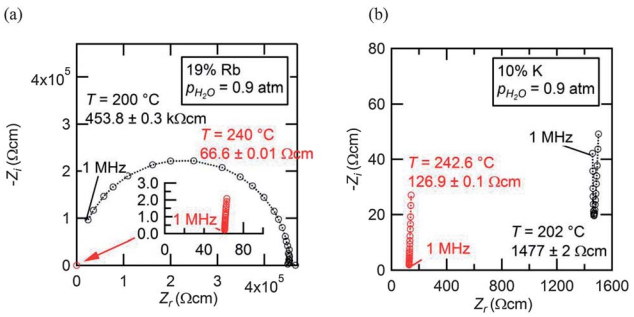

Fig. 14 AC impedance spectra collected from (a) $Cs_{0.81}Rb_{19}H_2PO_4$ and (b) $Cs_{0.90}K_{0.10}H_2PO_4$ at temperatures just below (black) and just above (red) the respective T_s values with $p_{H_2O} = 0.9$ atm. The behavior of $Cs_{0.81}Rb_{19}H_2PO_4$ is entirely analogous to that of neat CsH_2PO_4.[19] In the case of $Cs_{0.90}K_{0.10}H_2PO_4$, the surprisingly high conductivity below T_s results in a spectrum that has similar general characteristics to that above T_s, appearing as an almost vertical straight line with real intercept that corresponds to the bulk electrolyte conductivity.

introduction of K, the thermal signatures widen, particularly for $x = 0.2$ for the superprotonic transition and for both compositions for the dehydration event. These features in the $Cs_{1-x}K_xH_2PO_4$ system are tentatively assigned to wider compositional differences between phases in the two-phase regions. During the transformation from the monoclinic to cubic phase at small x, the finite heating rate used in the DSC experiments may, as a consequence of the necessary solid state diffusion, retard the transition and shift it to higher temperature than observed under the quasi-equilibrium conditions of the diffraction experiment. Similarly, gradual and continuous phase separation into distinct monoclinic and cubic phases or a potassium-rich liquid dehydrate [$MH_{2-2x}PO_{4-x}$(l)] and a cesium-rich solid may be responsible for the broadening observed in the thermal peaks.

3.4. Structural and transport properties

The thermal expansion behavior of the cubic phase in the $Cs_{1-x}Rb_xH_2PO_4$ and $Cs_{1-x}K_xH_2PO_4$ systems is summarized in Fig. 12 and Table 4, where the coefficients of thermal expansion, α, are of the form $\Delta a/a_0 = \alpha(T - T_0)$, with $T_0 = 260$ °C. These coefficients are approximately 4×10^{-5} K^{-1} for each of the compounds with negligible impact from the introduction of substituents. The volumetric expansion coefficient (3α) for CsH_2PO_4 in the cubic phase, determined here to be $1.57(3) \times 10^{-4}$ K^{-1}, is slightly smaller than that, $1.98(2) \times 10^{-4}$ K^{-1}, reported by Louie.[7] The lattice parameters measured in this work agree well with Louie's values and are slightly larger than those of other reports.[25–27] The influence of material composition, specifically, the weighted mean ionic radii,[28] on the cubic lattice parameter (at 260 °C) is summarized in Fig. 13. The data from the two systems show good agreement, indicating that the lattice constant of the solid-solution cubic phase depends simply on the averaged ionic radius of cations in the alkali ion site rather than the nature of the specific cation. Again, the behavior is in accord with Vegard's empirical law.

The AC impedance measurements revealed that the solid solution cubic phase has high conductivity in both the CsH_2PO_4–RbH_2PO_4 and the CsH_2PO_4–KH_2PO_4 systems. The impedance spectra at high temperature displayed typical features[19] in which the response appears as a straight line with a real intercept at the high frequency limit corresponding to the resistance of the polycrystalline solid electrolyte, Fig. 14. In the

Table 4 Thermal expansion coefficients ($\Delta a/a_0 = \alpha(T - T_0)$ with $T_0 = 260$ °C) of cubic $Cs_{1-x}Rb_xH_2PO_4$ and $Cs_{1-x}K_xH_2PO_4$

Composition	α (10^{-5} K^{-1})	a_0 (Å)	T (°C)	Composition	α (10^{-5} K^{-1})	a_0 (Å)	T (°C)
CsH_2PO_4	3.92(11)	4.9724(2)	230–290				
19%Rb	3.42(17)	4.9440(2)	230–280	3%K	3.95(13)	4.9675(2)	220–280
50%Rb	3.85(19)	4.8991(2)	240–270	15%K	4.54(48)	4.9388(8)	210–250
78%Rb	—	4.8612(3)	260	30%K	4.65(10)	4.9107(6)	210–250

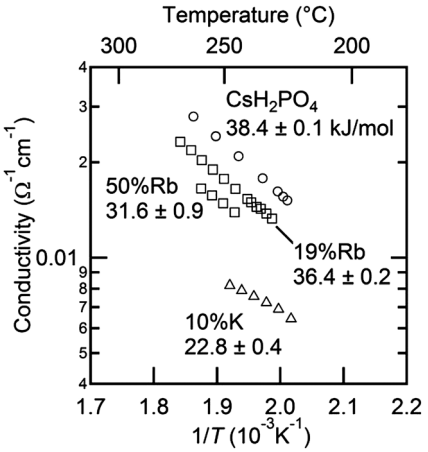

Fig. 15 Arrhenius representation of the conductivities of cubic $Cs_{1-x}Rb_xH_2PO_4$ and $Cs_{1-x}K_xH_2PO_4$ as functions of temperature.

case of the Rb containing compositions, the low temperature spectra were also typical of CsH_2PO_4, as shown for example for $Cs_{0.81}Rb_{0.19}H_2PO_4$, Fig. 14(a), in which the spectrum appears as a single, high-frequency arc, the diameter of which corresponds to the resistance of the electrolyte. The difference in conductivity at 200 and at 240 °C is almost four orders of magnitude, similar to the reported impact of the superprotonic transition on the transport properties of neat CsH_2PO_4. In contrast, the K containing compositions displayed surprisingly high conductivity even at temperatures below the transition, with the difference in conductivity between 202 and 243 °C being only about a factor of six for $Cs_{0.90}K_{0.10}H_2PO_4$. Although such enhancement is intriguing and results in spectra that are similar in the high and low temperature phases, Fig. 14(b), it was not explored further due to the overall low conductivity of the monoclinic phase. Moreover, measurements in the CsH_2PO_4–KH_2PO_4 system were limited to compositions lying within the solubility limit of potassium into monoclinic CsH_2PO_4 so as to eliminate any influence of ensemble microstructure. For comparative purposes, the conductivity of CsH_2PO_4 was also measured and was found to be in excellent agreement with literature values.[1,2,19,29]

Focusing on transport in the high temperature phase, Fig. 15, it is apparent that introduction of both Rb and K leads to a monotonic reduction of the conductivity of CsH_2PO_4. A similar result was observed by Matsuo,[9] but was reported without comment. Here, it is further observed that potassium has a stronger impact than rubidium. A close examination of the Arrhenius representation of the conductivity data reveals that, although the conductivity decreases on with increasing concentration of Rb or K, the activation energy for transport also decreases, and hence it is the reduction in the pre-exponential factor, A, in the expression $\sigma = \frac{A}{T}\exp\left(\frac{-E_a}{k_B T}\right)$ that correlates with the reduction in conductivity. A detailed investigation of the role of cation chemistry on proton transport characteristics is beyond the scope of the present work, which is instead focused on exploration of phase stability. Nevertheless, it is noteworthy that changes to the averaged structure apparently do not account for the change in transport properties. Specifically, although the cell volumes of $Cs_{0.81}Rb_{0.19}H_2PO_4$ and $Cs_{0.90}K_{0.10}H_2PO_4$ are almost identical, the latter has a conductivity that is less than half that of the former and an activation energy that is also almost halved in comparison, Table 5. Elucidation of the origins of this intriguing phenomenon awaits a future study.

Table 5 Activation energy and pre-exponential factor for proton transport in cubic $Cs_{1-x}Rb_xH_2PO_4$ and $Cs_{1-x}K_xH_2PO_4$

Composition	E_a (eV)	$\log(A)$ Ω^{-1} cm^{-1} K
CsH_2PO_4	38.4 ± 0.1	11.32 ± 0.02
19%Rb	36.4 ± 0.2	10.60 ± 0.05
50%Rb	31.6 ± 0.9	9.31 ± 0.20
10%K	22.8 ± 0.4	6.73 ± 0.08

4. Conclusions and summary

The results of this work are summarized as follows. The CsH_2PO_4–RbH_2PO_4 system displays complete solid solubility at all temperatures above 180 °C. The transformation from the monoclinic phase ($P2_1/m$) to the superprotonic cubic phase ($Pm\bar{3}m$) shifts to higher temperatures with increasing Rb content. Simultaneously, the dehydration temperature largely decreases, resulting in a narrowing of the region of stability of the cubic phase. In the case of the end-member RbH_2PO_4 compound, this phase cannot be observed under 1 atm p_{H_2O}. While a two-phase region is expected between the monoclinic and cubic phases at intermediate composition, the width of this region is too small for detection in this study. In contrast, CsH_2PO_4–KH_2PO_4 forms a eutectoid system, with a eutectoid temperature of ~208 °C. The solubility limit of K into cubic CDP is 27 at.% and is surprisingly temperature insensitive above the eutectoid temperature up to 260 °C. Below the eutectoid point the solubility drops steeply. Within the single-phase cubic region, the transition temperature decreases monotonically, but is accompanied by a simultaneous decrease in the dehydration temperature. Thus, the phase stability width of the superprotonic phase is relatively unchanged upon introduction of K. The phase boundaries could not be accurately determined due to the challenges of high temperature, *in situ* composition measurements and the slow equilibration kinetics. A wider two-phase region between monoclinic and cubic phases than the Rb system is inferred on the basis of the broader DSC signals.

In both systems, the cubic cell volume decreases in proportion to the substituent concentration. The reduction is independent of the nature of the element, instead being given by the average cation radius. The thermal expansion coefficient in the cubic phase is, within the limits of measurement, independent of composition.

The most significant finding is the substantial reduction in conductivity in the high-temperature cubic phase upon introduction of substituent elements. This reduction occurs as a result of a dramatic decrease in the pre-exponential factor. Furthermore, the influence of K on the conductivity exceeds that of its influence on the cell volume, suggesting that the impact on transport must be due to local rather than global or averaged effects. The reduction in conductivity due to the

introduction of substituent elements, though undesirable from a technological perspective, provides a possible avenue for elucidating and ultimately tuning the rate-limiting step in charge transport in superprotonic crystals. At this stage, unmodified CsH_2PO_4 remains the most feasible composition for fuel cell development.

Acknowledgements

The authors gratefully acknowledge financial support from U.S. National Science Foundation, Division of Materials Research (DMR-0906543) and the Army Research Office MURI Program (W911NF-07-1-0410).

References

1 D. A. Boysen, T. Uda, C. R. I. Chisholm and S. M. Haile, *Science*, 2004, **303**, 68–70.
2 J. Otomo, T. Tamaki, S. Nishida, S. Q. Wang, M. Ogura, T. Kobayashi, C. J. Wen, H. Nagamoto and H. Takahashi, *J. Appl. Electrochem.*, 2005, **35**, 865–870.
3 T. Uda, D. A. Boysen, C. R. I. Chisholm and S. M. Haile, *Electrochem. Solid-State Lett.*, 2006, **9**, A261–A264.
4 A. Ikeda and S. M. Haile, *Solid State Ionics*, 2012, **213**, 63–71.
5 Y. Uesu and J. Kobayashi, *Phys. Status Solidi A*, 1976, **34**, 475–481.
6 A. R. Al-Karaghouli, B. Abdul-Wahab, E. Ajaj and A. Sequeira, *Acta Crystallogr., Sect. B: Struct. Crystallogr. Cryst. Chem.*, 1978, **34**, 1040–1042.
7 M. W. Louie, M. Kislitsyn, K. Bhattacharya and S. M. Haile, *Solid State Ionics*, 2010, **181**, 173–179.
8 L. Cowan, Ph.D. Thesis, California Institute of Technology, Pasadena, California, 2007.
9 Y. Matsuo, J. Hatori, Y. Yoshida and S. Ikehata, *Solid State Ionics*, 2012, **213**, 42–44.
10 C. E. Botez, H. Martinez, R. J. Tackett, R. R. Chianelli, J. Z. Zhang and Y. S. Zhao, *J. Phys.: Condens. Matter*, 2009, **21**, 325401.
11 G. V. Lavrova, V. V. Martsinkevich and V. G. Ponomareva, *Inorg. Mater.*, 2009, **45**, 795–801.
12 A. Ikeda and S. M. Haile, *Solid State Ionics*, 2010, **181**, 193–196.
13 V. V. Martsinkevich, V. G. Ponomareva, T. N. Drebushchak, G. V. Lavrova and S. S. Shatskaya, *Inorg. Mater.*, 2010, **46**, 765–769.
14 C. E. Botez, R. J. Tackett, J. D. Hermosillo, J. Z. Zhang, Y. S. Zhao and L. P. Wang, *Solid State Ionics*, 2012, **213**, 58–62.
15 H. Naili, N. Zouari, T. Mhiri and A. Daoud, *J. Mol. Struct.*, 2000, **519**, 143–151.
16 K. Itoh and M. Uchimoto, *Ferroelectrics*, 1998, **217**, 155–162.
17 C. E. Botez, D. Carbajal, V. A. K. Adiraju, R. J. Tackett and R. R. Chianelli, *J. Phys. Chem. Solids*, 2010, **71**, 1576–1580.
18 D. A. Boysen, S. M. Haile, H. J. Liu and R. A. Secco, *Chem. Mater.*, 2004, **16**, 693–697.
19 S. M. Haile, C. R. I. Chisholm, K. Sasaki, D. A. Boysen and T. Uda, *Faraday Discuss.*, 2007, **134**, 17–39.
20 F. Izumi and K. Momma, *Applied Crystallography XX*, 2007, **130**, 15–20.
21 B. N. Dutta, *Phys. Status Solidi B*, 1962, **2**, 984–987.
22 M. Komukae, K. Kawashima and T. Osaka, *J. Phys. Soc. Jpn.*, 2000, **69**, 2076–2081.
23 P. W. Atkins and J. de Paula, *Physical chemistry*, Oxford University Press, 8th edn, 2006.
24 C. R. I. Chisholm, Ph.D. Thesis, California Institute of Technology, 2003.
25 K. Yamada, *Solid State Ionics*, 2004, **175**, 557–562.
26 W. Bronowska, *Mater. Sci.-Pol.*, 2006, **24**, 229–236.
27 A. Preisinger, K. Mereiter and W. Bronowska, *Mater. Sci. Forum*, 1994, **166**, 511–516.
28 L. Pauling, *The Nature of the Chemical Bond*, Cornell University Press, 1960.
29 A. Ishikawa, H. Maekawa, T. Yamamura, Y. Kawakita, K. Shibata and M. Kawai, *Solid State Ionics*, 2008, **179**, 2345–2349.

